CHAPTER 6

IMPROVEMENT OF TRIBO-ACTIVE BEHAVIOR OF g-C_3N_4 NANOSHEETS USING m-$LAVO_4$ NANOPARTICLES

A graphitic carbon nitride, g-C_3N_4, is considered the most stable allotrope of carbon nitride and possesses a two-dimensional structure stacked by weak van der Waals interactions. Metal-free polymer g-C_3N_4 comprises mainly carbon, nitrogen, and traces of hydrogen. Its two-dimensional aromatic tri-s-triazine structure exhibits various properties, such as high thermal stability and chemical stability, besides excellent mechanical, electronic, and optical properties [Gaddam et al. (2020), Wu et al. (2019), Liu et al. (2019), Wen et al. (2017)]. Furthermore, its low cost, easy availability, and eco-friendly nature make it to apply in various fields such as photoreduction of CO_2 [Li et al. (2018)], solar cells [Jiang et al. (2018)], bioimaging[Zhang et al. (2013)], supercapacitors [Ghaemmaghami et al. (2019)], fluorescence sensors [Zhang et al. (2014)], photocatalytic degradation of organic wastewater [Gao et al. (2018)], photoelectrochemical cathodic protection [Jing et al. (2021)], photocatalysts for water disinfection [Zhang et al. (2019)], microbial control [Zhang et al. (2019)], photocatalytic hydrogen evolution [Zhu et al. (2021)], batteries [Weng et al. (2019)], H_2O_2 synthesis [Feng et al. (2020)] and SERS detection [Tang et al. (2020)], etc. In addition, g-C_3N_4 nanosheets have been utilized as nano additives in lubrication [Kumar et al. (2017)]. Under the sliding motion, weak van der Waals interactions between the neighboring layers enhance shearing [Shukla et al. (2020), Singh et al. (2021)]. The antiwear properties of bulk graphitic carbon nitride with polyvinylidene difluoride were reported by Zhu et al. [Zhu et al. (2020)]. Kumar and his associates reported the antifriction/antiwear behavior of octadecyl amine grafted g-C_3N_4 nanosheets [Kumar et al. (2017)]. The tribological activity of nanocomposite g-C_3N_4/MoS_2 was studied by Xu et al. [Xu et al. (2018)]. Yang and his co-workers investigated the tribological properties of nanocomposite, including copper nanoparticles and g-C_3N_4 as an additive to paraffin base oil [Yang et al. (2015)]. Min et al. found the antifriction nature of a

composite consisting of copper nanoparticles and polydopamine-functionalized oxygenated nanosheets (g-C_3N_4) [Min et al. (2020)]. The antiwear behavior of polyimide was improved by Wu and collaborators using CuO/g-C_3N_4 composite [Wu et al. (2019)]. They also investigated the tribo-active behavior of phenolic coating with varying percentages of g-C_3N_4 nanosheets [Wu et al. (2019)]. Zhang and his associates reported the antiwear properties of g-C_3N_4/TiO_2 nanocomposite [Zhang et al. (2019)]. Recently, nanohybrid, N−ZnO/g-C_3N_4, has been used as the friction and wear modifier of paraffin oil at 0.20 % w/v in our laboratory [Singh et al. (2021)].

Lanthanum orthovanadate ($LaVO_4$) has been used in numerous fields, such as lasers host materials [Sun et al. (2013)], phosphors [Rai et al. (2020)], bioimaging [Jeyaraman et al. (2016)], luminescent materials [Wang et al. (2012)], and catalysts/ photocatalysts [Paunović et al. (2018), Shafiq et al. (2021)], owing to its properties such as redox, electronic, optical, vibrational, nontoxicity, thermal and chemical stability [Paunović et al. (2018), Sun et al. (2010), Vairapperumal et al. (2020)]. Several vanadates, like silver vanadate (Ag_3VO_4) [Singh et al. (2010), Luster et al. (2011)] and cerium orthovanadate $CeVO_4$ [Fengzhen et al. (2011)], have been used in the field of lubrication. Lanthanum orthovanadate has two polymorphic phases, monoclinic and tetragonal, denoted as m-; monazite and t-; zircon-type crystal structure, respectively. $LaVO_4$ in the monazite form is in a thermodynamically stable state. Lanthanum ion imposes significant inclination in the direction of m-monazite type structure due to its larger ionic radius and higher oxygen coordination number (nine) [Sun et al. (2010), Yamuna et al. (2021)]. Therefore, m-$LaVO_4$ has been synthesized by solution combustion method using glycine as a fuel [Veldurthi et al. (2018)].

Liu and his associates explained the photocatalytic water-splitting activity of

nanocomposite, $LaVO_4/g\text{-}C_3N_4$ [Liu et al. (2021)]. A hydrothermally synthesized nanocomposite of $LaVO_4$ with red carbon nitride (rod-like) has been applied for the photodegradation of antibiotics under visible light by Jing et al. [Jing et al. (2020)]. Li and his co-workers recently published a paper using $LaVO_4/C_3N_4$ for photocatalytic H_2 evolution and high-value-added furfural production [Li et al. (2022)]. Khalid and his group have reported mesoporous $LaVO_4/C_3N_4$ as a photocatalyst for the mineralization of trichloroethylene [Mkhalid et al. (2022)]. He et al. studied the photocatalytic activity of composites $m\text{-}LaVO_4/g\text{-}C_3N_4$ and $t\text{-}LaVO_4/g\text{-}C_3N_4$ [He et al. (2014)].

In the present work, $g\text{-}C_3N_4$ nanosheets, $m\text{-}LaVO_4$ nanoparticles, and binary nanocomposite, $g\text{-}C_3N_4/m\text{-}LaVO_4$, have been prepared. The nano additives could be examined through FT-IR, p-XRD, TEM, HR-SEM, and XPS. The tribological activity of these nano additives has been evaluated in paraffin oil (PO) at 0.05 % w/v optimized concentration under test conditions (ASTM D4172 and ASTM D5183) on a four-ball tester**.**

6.1. Materials and Methods

6.1.1. Chemicals for utilization

Ammonium metavanadate; NH_4VO_3, lanthanum nitrate hexahydrate; $La(NO_3)_3.6H_2O$, melamine, and glycine were procured from Sigma-Aldrich. Paraffin oil was obtained from Qualigens Fine Chemicals.

6.1.2. Synthesis of various additives

6.1.2.1 Synthesis of graphitic carbon nitride nanosheets

Melamine was heated to prepare the $g\text{-}C_3N_4$ powder. 5 g of melamine was placed in an alumina crucible with a lid and calcined for four hours at 550 °C in a muffle furnace. The product was removed from the crucible when cooled to room temperature. Further, it was ground to provide graphitic carbon nitride powder. For 3-4 hours, the powder was ultrasonicated in 100 mL of a

50 percent $C_2H_5OH–H_2O$ mixture. The resulting colloidal suspension was centrifuged at 4000 rpm for 15 minutes to sediment the bigger particles. The supernatant portion of the solution was taken, and the solvent was evaporated and finally dried to produce nanosheets; g-C_3N_4 [Singh et al. (2021)].

6.1.2.2. Preparation of monazite lanthanum orthovanadate (m-$LaVO_4$)

A solution combustion method has been used to prepare m-$LaVO_4$ using glycine as fuel. 1.705 g of lanthanum nitrate hexahydrate and 0.46 g ammonium metavanadate were dissolved in 15 mL of distilled water and 3 M HNO_3 (5 mL). In a combustion petri dish, the solutions were mixed thoroughly and agitated with a magnetic stirrer. In 10 mL of distilled water, 0.55 g of glycine was dissolved and added to the reaction mixture. The prepared solution mixture was placed into a muffle furnace at 400 °C for 20 minutes. Finally, the resultant product was calcined at 500 °C for 2.5 h in a muffle furnace to get the pure m-$LaVO_4$ nanoparticles [Veldurthi et al. (2018)].

6.1.2.3. Preparation of nanocomposite (g-C_3N_4/m-$LaVO_4$)

Carbon nitride, g-C_3N_4 nanosheets (0.2 g), and monazite lanthanum vanadate (0.2 g) were dispersed in ethanol separately and sonicated for 1h using an ultrasonic probe at about 50 °C. Both were mixed and sonicated at 70 °C. The obtained material was filtered, dried, and then placed in a microwave oven for 3 - 4 min at 700 Watts to yield g-C_3N_4/m-$LaVO_4$ (**Fig. 6.1**).

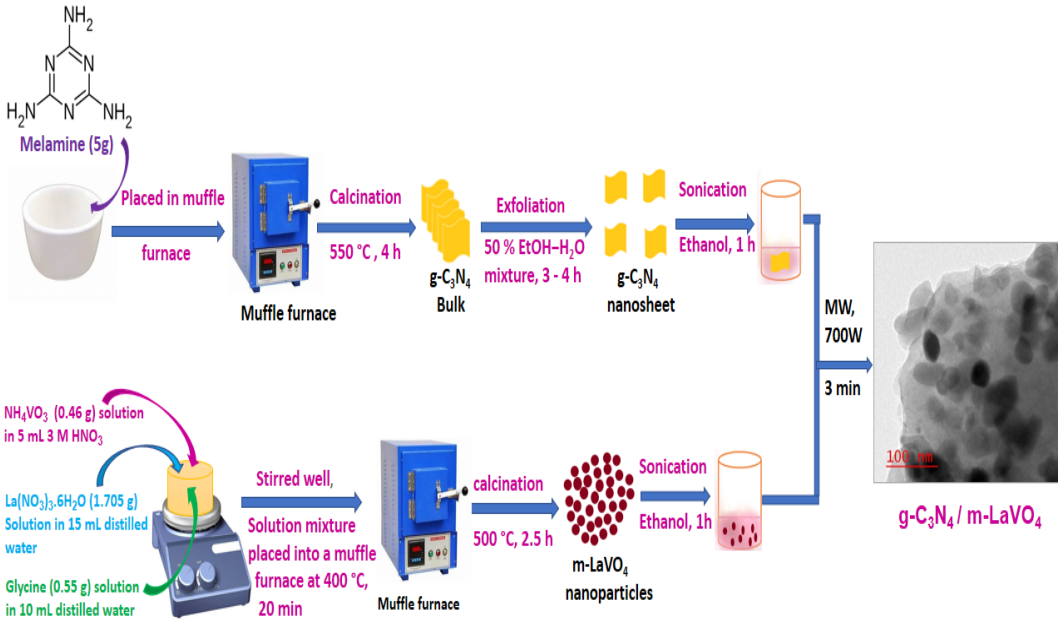

Fig. 6.1. Illustration of nanocomposite (g-C_3N_4 / m-$LaVO_4$) preparation

6.2. The characterization techniques for nano additives

The characterization of lubricant additives has been performed by various techniques such as HR-SEM, HR-TEM, TEM, FTIR, p-XRD, and XPS.

6.3. Triblogical tests procedure

Using 1h of sonication at room temperature, test samples of the additives with various concentrations were made in base oil; 0.000, 0.025, 0.050, 0.100, 0.150, and 0.200 percent w/v. The tribological activity of the prepared samples was evaluated according to ASTM D4172 test conditions. The optimized concentration of the nano additives was established as 0.05 % w/v from the observed data. The ASTM D5183 test conditions were used to conduct load ramp testing for nano lubricants.

6.4. Results and Discussion

6.4.1. Characterization of the prepared additives

HR-SEM was used to investigate the shape and microstructure of the additives; g-C_3N_4 nanosheets, m-$LaVO_4$ nanoparticles, and nanohybrid (g-C_3N_4/m-$LaVO_4$). The resultant images are presented in **Fig. 6.2** (a-c), respectively. The arbitrarily piled fluffy graphitic carbon nitride nanosheets are visible in **Fig. 6.2a**. The lateral size of nanosheets lies in the range of 180 -1200 nm with a thickness of 10-15 nm [Singh et al. (2021)]. The lubricating behavior is influenced by the size and thickness of the nanosheets. The thinner the nanosheets, the better they penetrate the sliding interfaces [Shukla et al. (2020)]. **Fig. 6.2b** shows that m-$LaVO_4$ consists of an aggregation of almost spherical nanoparticles [Veldurthi et al. (2018)]. Nanosheets, g-C_3N_4 furbished with m-$LaVO_4$ nanoparticles are depicted in **Fig. 6.2c.** The EDX analysis of nanohybrid, g-C_3N_4 /m-$LaVO_4$ is displayed in **Fig. 6.2c'**, showing the presence of all elements of nanocomposite such as carbon, nitrogen, oxygen, lanthanum, and vanadium, verifying the formation of the composite; g-C_3N_4/m-$LaVO_4$.

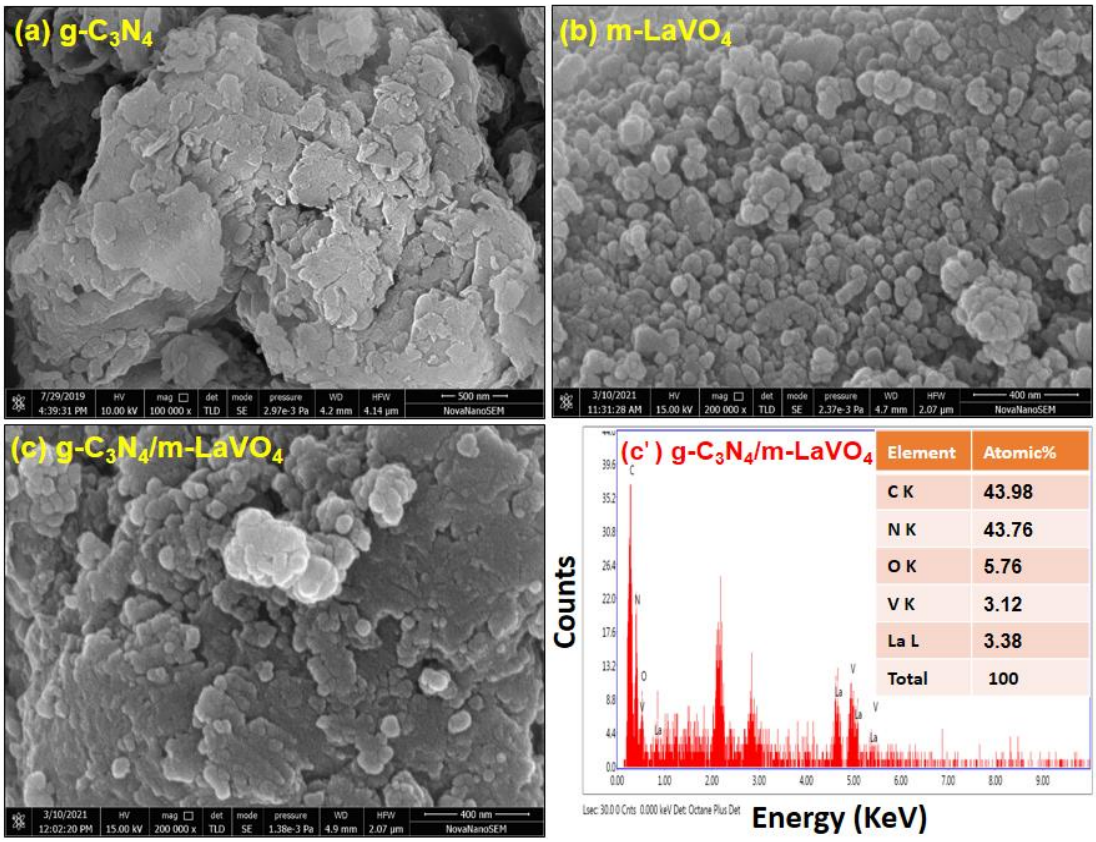

Fig. 6.2. (a-c) HR-SEM images of nano additives and (c') EDX spectrum of g-C_3N_4/m-$LaVO_4$

For a better understanding of their morphology, TEM images of g-C_3N_4nanosheets, m-$LaVO_4$ nanoparticles, and nanocomposite (g-C_3N_4/m-$LaVO_4$) have been provided and displayed in **Fig. 6.3(a-c)**, respectively. The lamellar structure of graphitic carbon nitride can be observed in **Fig**. **6.3a**. The TEM micrograph of m-$LaVO_4$ nanoparticles in **Fig 6.3b** also confirms an almost spherical shape. **Fig. 6.3a'** shows the HR-TEM image of g-C_3N_4 nanosheets. The d- spacing of the nanosheet was found to be 0.324 nm, which corresponds to the (002) plane [Singh et al. (2021), Kong et al. (2017)]. The HR-TEM image of nanoparticles can be seen in **Fig 6.3b'**. Furthermore, the SAED pattern of m-$LaVO_4$ nanoparticles shows crystalline nature. The d- spacing for m-$LaVO_4$ could be found as 0.320 nm, corresponding to

to the (120) plane [Veldurthi et al. (2018)].

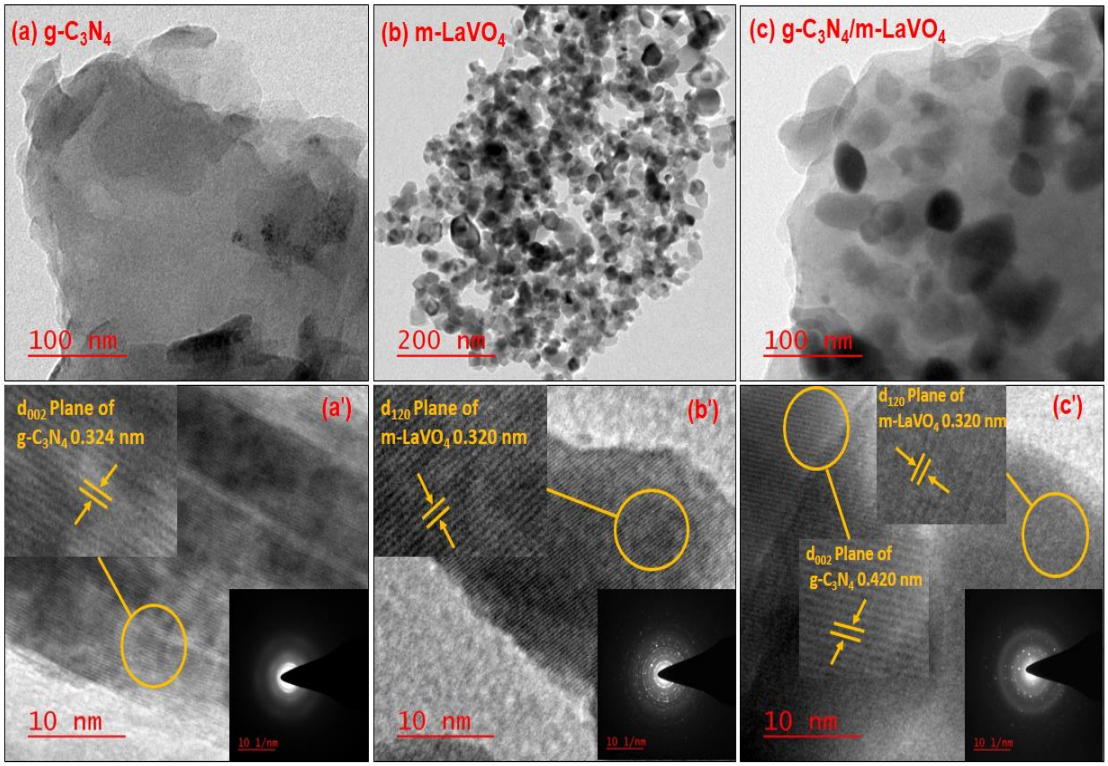

Fig. 6.3. TEM images of (a) g-C_3N_4 nanosheets (b) m-$LaVO_4$ nanoparticles (c) g-C_3N_4/m-$LaVO_4$ composite, HR-TEM images (a') g-C_3N_4 nanosheets (b') m-$LaVO_4$ nanoparticles, and (c') g-C_3N_4/m-$LaVO_4$ composite, SAED patterns of the lubricant additives shown in the inset view (a', b', c')

Figs. 6.3c and **6.3c'** show TEM and HR-TEM micrographs of the nanocomposite g-C_3N_4/m-$LaVO_4$, respectively. The interplanar spacing of nanosheets corresponding to the plane (002) increases from 0.324 nm to 0.420 nm in the composite. The increase in interplanar spacing corresponding to the (002) plane in nanosheets indicates that m-$LaVO_4$ nanoparticles have interacted very well with the nanosheets.

The particle size distribution histogram for nanoparticle (m-$LaVO_4$) could be obtained from TEM analysis and presented in **Fig. 6.4**. According to that, 27.5 nm could be considered the average nanoparticle size.

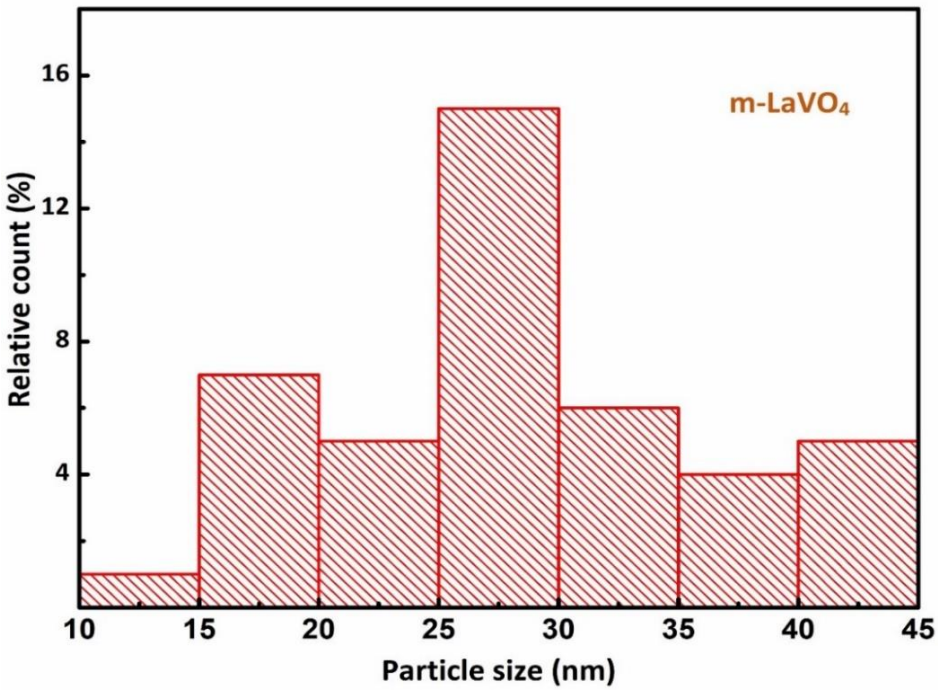

Fig. 6.4. The particle size histogram for m-$LaVO_4$ obtained from TEM studies

The XRD patterns of nanosheets, nanoparticles, and nanocomposite are displayed in **Fig. 6.5a**. The diffraction pattern of g-C_3N_4 nanosheets follows JCPDS No. 87-1526. Accordingly, the peak at 13.0° corresponds to the characteristic peak of interlayer separation assigned to the (100) plane; however, the peak at 27.5° corresponds to the distinct peak of interplanar stacking assigned to the (002) plane [Singh et al. (2021), Iqbal et al. (2022)]. The XRD pattern of m-$LaVO_4$ follows JCPDS No. 70-0216, confirming its monoclinic structure [Veldurthi et al. (2018)]. The absence of extra peaks authenticates a single phase for m- $LaVO_4$. The nanocomposite g-C_3N_4/m-$LaVO_4$ exhibits all characteristic diffraction peaks, indicating

the coexistence of both g-C_3N_4 and m-$LaVO_4$ together.

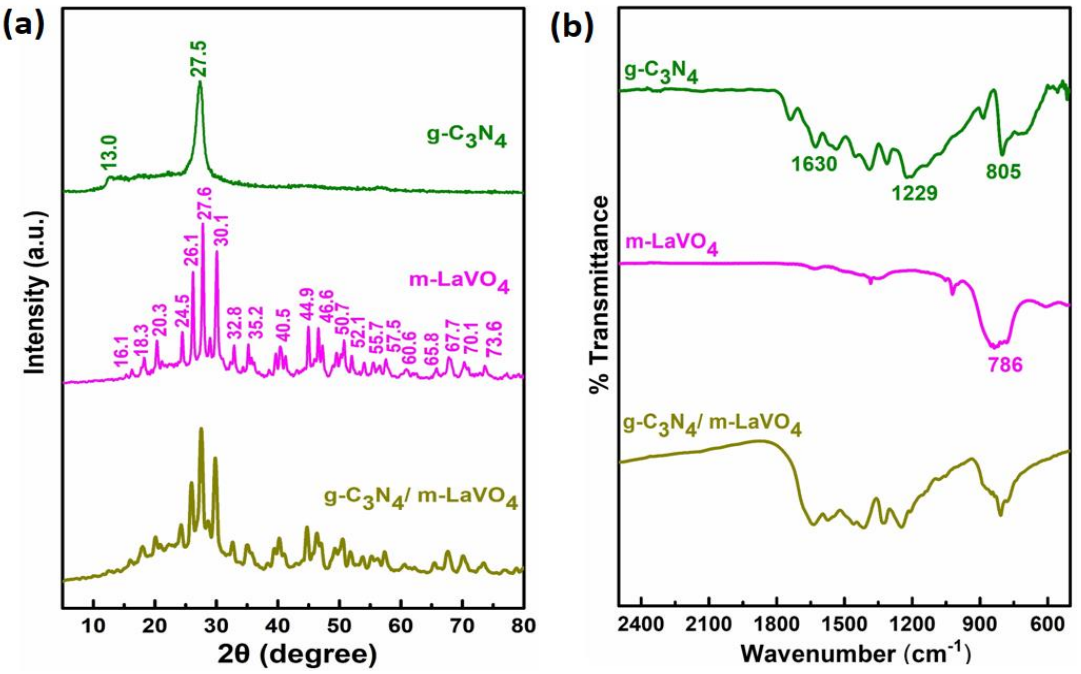

Fig. 6.5. (a) XRD spectra of synthesized g-C_3N_4 nanosheets, m-$LaVO_4$ nanoparticles, g-C_3N_4/m-$LaVO_4$ composite, and (b) FT-IR spectra of g-C_3N_4 nanosheets, m-$LaVO_4$ nanoparticles, g-C_3N_4/m-$LaVO_4$ composite

FT-IR has been used to identify different functional groups in lubricant additives, as displayed in **Fig. 6.5b**. The spectrum of the nanosheets shows the characteristic peak at 805 cm^{-1}, 1229 $cm^{-1,}$ and 1630 $cm^{-1,}$ corresponding to breathing mode vibration of the s-triazine ring, C−N, and C=N stretching frequencies, respectively [Singh et al. (2021), Kong et al. (2017)]. The absorption peak at 786 cm^{-1} in the spectrum of m-$LaVO_4$ is assigned to the stretching mode of the V-O of the VO_4^{3-} group [Li et al. (2020)]. Moreover, the presence of all the peaks due to g-C_3N_4 and m-$LaVO_4$ in the spectrum of the nanocomposite validates its formation.

The XPS analysis has been utilized to recognize the chemical states of all the constituent elements present in nanohybrid (g-C_3N_4/m-$LaVO_4$). Using peak fit software, **Fig. 6.6(a-e)** presents core-level spectra of C 1s, O 1s, N 1s, V 2p, and La 3d, respectively. **Fig. 6.6a** shows the C 1s core-level spectrum, indicating two peaks: C–C/C=C (284.6 eV) and N–C=N (287.9 eV) [Kavita et al. (2020), Singh et al. (2021)]. **Fig. 6.6b** depicts the O 1s spectrum, showing a peak at binding energy 530.4 eV, corresponding to the V-O bond from VO_4^{3-} [He et al. (2014), Zou et al. (2020)].

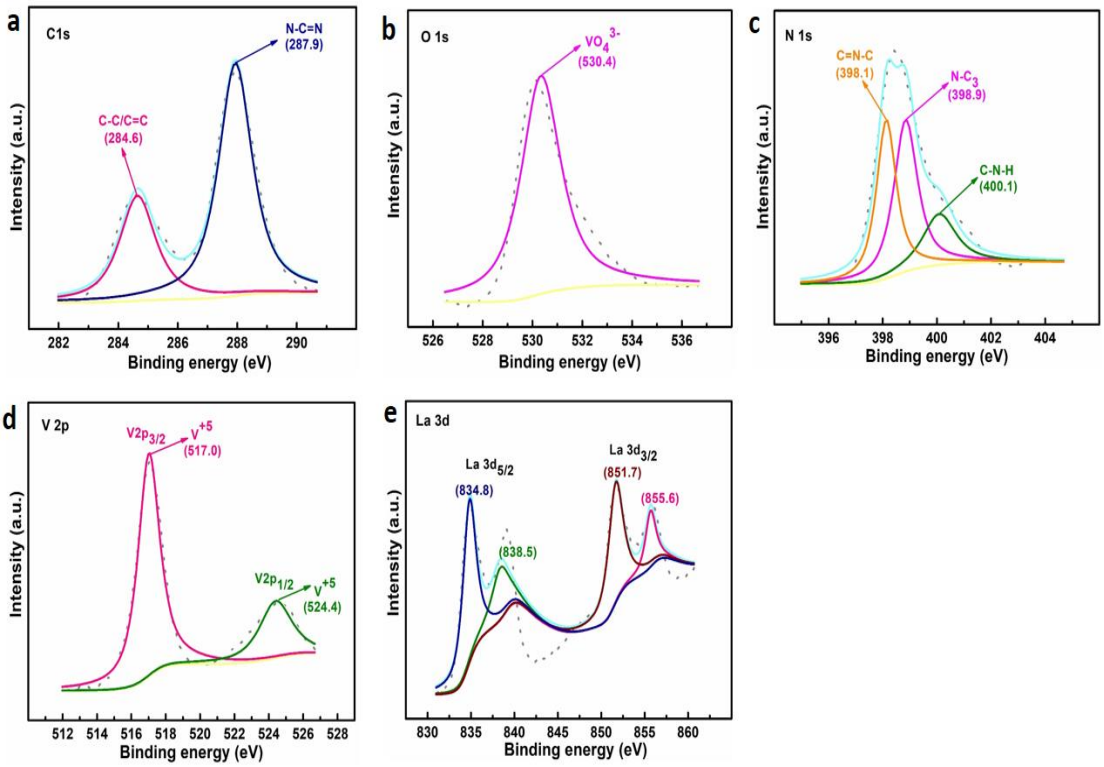

Fig. 6.6. XPS spectra of nanocomposite g-C_3N_4/m-$LaVO_4$.

Fig. 6.6c describes the N 1s spectrum, where three peaks with binding energies of 398.1, 398.9, and 400.1 eV are observable due to C-N=C, N-C_3, and C-N-H, respectively [Tan et al. (2017)]. The two peaks with binding energies of 517.0 and 524.4 eV, corresponding to V $2p_{3/2}$ and V

$2p_{1/2,}$ respectively, could be identified [Li et al. (2022)] in the core-level spectrum of V 2p, **Fig. 6.6d**, indicating the presence of V^{+5} ion in the composite. **Fig. 6.6e** illustrates the La 3d spectrum, showing four peaks with binding energies of 834.8 and 838.5 eV for La $3d_{5/2}$ and 851.7 and 855.6 eV for La $3d_{3/2}$ [Li et al. (2022)].

6.4.2. Tribological Properties

6.4.2.1. Determination of dispersion stability of nanofluids

The dispersions sustainability of nanofluids is mainly desirable for tribo-active materials. The nano lubricants dispersions containing an optimized concentration of the additives (0.050 % w/v) were made using the ultrasonic probe, and then these were diluted ten times with paraffin oil. The UV-Vis spectra of the dispersions were recorded in the range of 250−800 nm every 12 hours within 48 hours. The change in relative absorbance vs. settling time for the prepared lubricating additives is shown in **Fig. 6.7a**. Generally, the relative absorbance value has gone down with time, but it was noticed that the amount of decrement is small for all the additives. Furthermore, the minimum settling was observed in the presence of composite g-C_3N_4/m-$LaVO_4$. The photographs of admixtures of g-C_3N_4, m-$LaVO_{4,}$ and composite g-C_3N_4/m-$LaVO_4$ additives in base oil were taken initially and after 48 hours, as displayed in **Fig. 6.7b**.

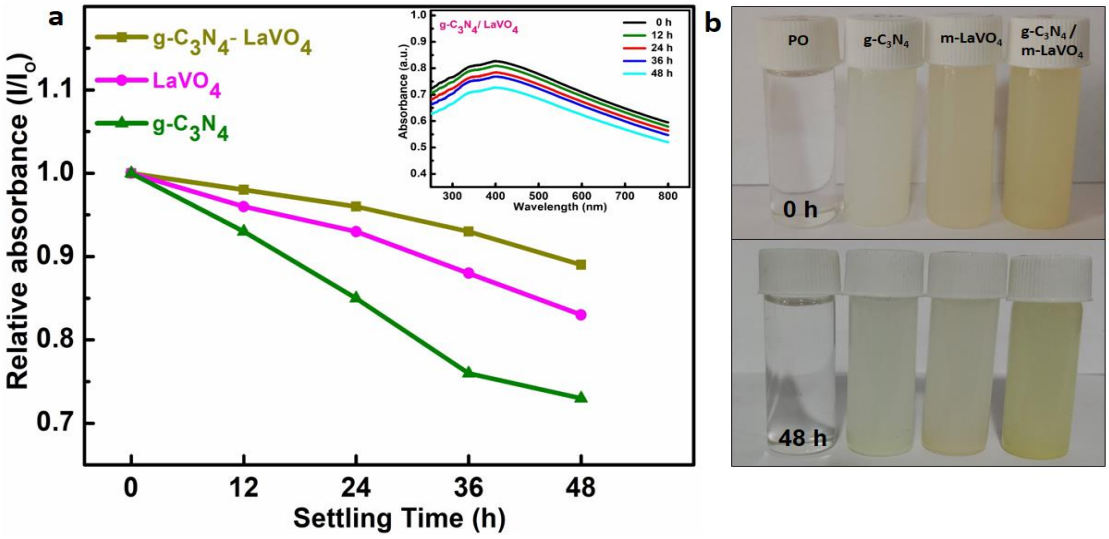

Fig. 6.7. (a) UV-visible spectrophotometry for evaluation of dispersion stability of blends of g-C_3N_4 nanosheets, m-$LaVO_4$ nanoparticles, and g-C_3N_4/m-$LaVO_4$ in PO (b) optical images of the lubricant additives dispersed in paraffin oil at 0 and 48 h

6.4.2.2. Wear and friction studies(ASTM D4172Test)

Because the concentration parameter influences the tribological characteristics of nano additives, concentration optimization has been done before commencing the tribological experiments. **Fig. 6.8a** shows the variation of mean wear diameter (MWD) as a function of nano additives concentration in the range 0.025-0.200 % w/v at 392 N applied load; 1200 rpm; 60 min test duration; 75 ^oC temperature in the base oil. MWD values are considerably reduced by adding nano additives in paraffin oil at each concentration, as shown in **Fig. 6.8a**, compared to PO alone The degree of decline is most significant for the composite g-C_3N_4/m-$LaVO_4$ and least for g-C_3N_4 nanosheets at each concentration. Initially, at 0.025 percent w/v, the MWD values for each additive were lower than that of base oil (0.735 mm). The lowest values of MWD are observed for the composite at 0.050 % w/v, for m-$LaVO_4$ at 0.100 % w/v, and for

g-C_3N_4 at 0.150 % w/v. After the lowest values, MWD increases linearly up to 0.200 % w/v in each case. As a result, the optimized concentration for conducting tribological activity tests has been determined to be 0.050 % w/v.

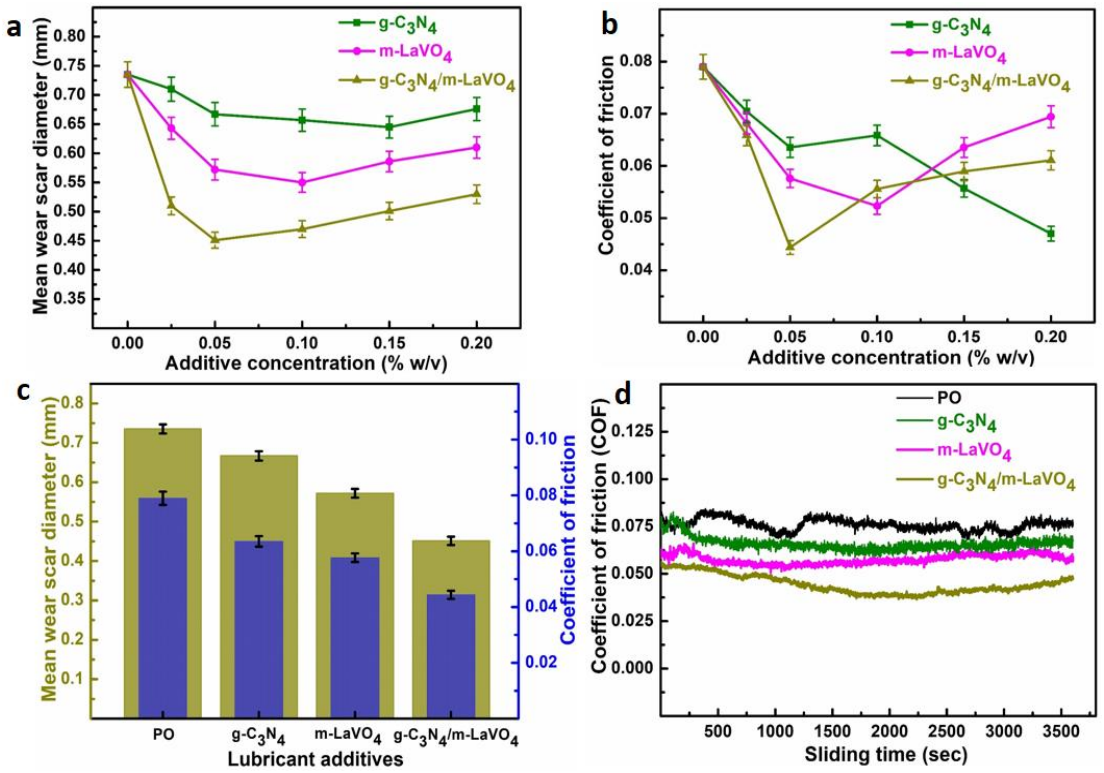

Fig. 6.8. ASTM D 4172 test for PO with and without additives (a) Optimization of the concentration of nano additives, (b) Alteration of COF vs. nano additives concentration, (c) Bar diagram showing average COF and MWD, (d) Alteration of the COF with sliding time

The variation in coefficient of friction (COF) with nano additives concentration is displayed in **Fig. 6.8b.** For base oil, the value for COF is very high, which reduces significantly in the presence of nano additives. It is observed that the COF value at 0.025 % w/v concentration for each nano additive is lowered considerably. The COF reduction continues

regularly up to 0.050 % w/v for all the additives. In the case of g-C_3N_4, COF increases slightly at the next concentration of 0.100 % w/v; beyond that, it decreases continuously up to 0.200 % w/v. The additive m-$LaVO_4$ shows a further decrease of COF at 0.100 % w/v but increases thereafter. However, there is an increase of COF for the composite throughout after 0.050 % w/v. Thus, the lowest COF values have been obtained as 0.04701 for g- C_3N_4 (at 0.200 % w/v), 0.05231 for m-$LaVO_4$ (at 0.100 % w/v), and 0.04438 (at 0.050 % w/v) for g-C_3N_4/m-$LaVO_4$,

The test conditions (ASTM D4172) have been applied to determine the antiwear/antifriction efficiency of the additives. **Fig. 6.8c** shows the test outcome in bar diagram form, showing MWD and COF simultaneously at the optimized concentration of 0.050 percent w/v. The MWD value of base oil, 0.735 mm, has undergone substantial reduction, g-C_3N_4 (9.3 %), m-$LaVO_4$ (22.2 %), and g-C_3N_4/m-$LaVO_4$ (38.6 %). It is clearly shown from the data mentioned above that a decrease in MWD value is directly related to their antiwear properties. Hence, the composite (g-C_3N_4/m-$LaVO_4$) has improved the antiwear behavior much better than g-C_3N_4 nanosheets or m-$LaVO_4$ nanoparticles.

Fig. 6.8d describes the alteration in COF of base oil in the presence and absence of lubricant additives vs. sliding time. The average value of COF for base oil, 0.0790, has experienced a reduction of 19.6 % for g-C_3N_4; 27.01 % for m-$LaVO_4$, and finally for composite g-C_3N_4/m-$LaVO_4$; 43.8 %. As expected, the value of COF is initially high in each case because tribochemical interaction has not yet begun to generate tribofilm. As time passes, tribofilm is formed, resulting in COF stabilization.

6.4.2.3. Load Carrying capacity (ASTM D 5183 test)

The load-carrying capacity of paraffin oil and its admixtures with lubricant additives were evaluated using test conditions ASTM D5183 at 0.050 % w/v (optimized concentration). At first, the running-in period was completed following the test conditions; 392 N load, 600 rpm,

75 °C temperature, and 60 min duration. Further, the steady-state test was continued with a 98 N load added every 10 min until the seizure load, which denotes the failure of lubricant additives to bear that load due to excessive frictional torque. **Fig. 6.9** shows the alteration in frictional torque vs. stepwise load and sliding time for base oil in the presence and absence of additives. The figure shows that base oil fails at a 1078 N load, but admixtures fail at much higher loads; g-C_3N_4 (1372 N), m-$LaVO_4$ (1764 N), and the nanocomposite g-C_3N_4/m-$LaVO_4$; (3136 N).

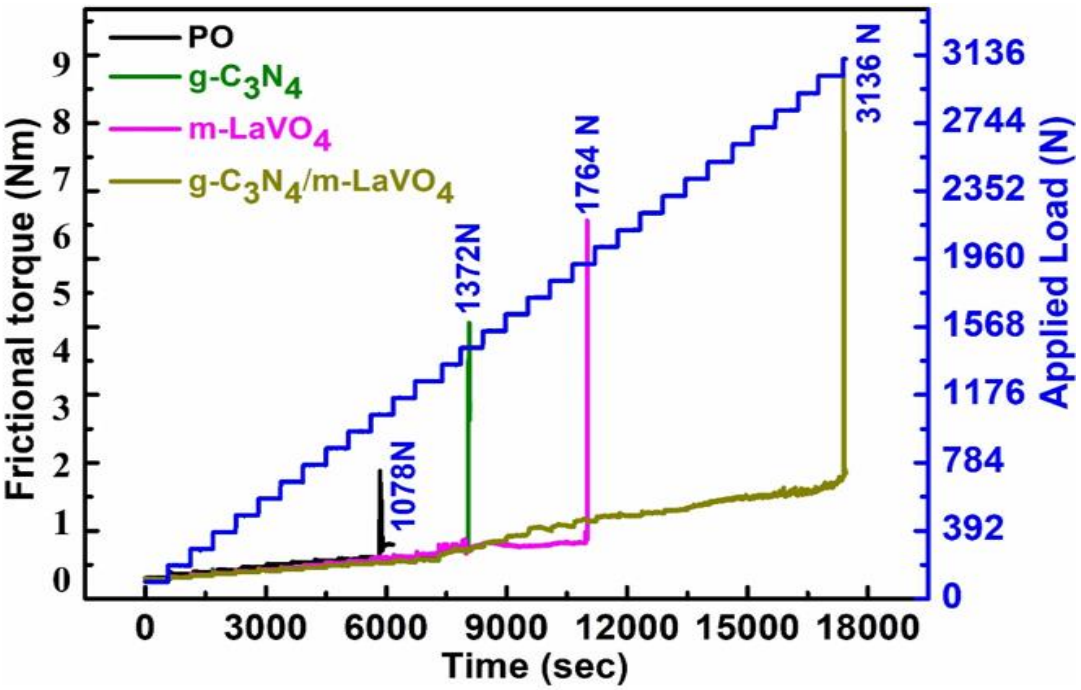

Fig. 6.9. Changes in frictional torque against stepwise loading and sliding time under ASTM D5183 test standards for PO with and without lubricant additives at 0.05 % w/v concentration

6.4.2.4. Determination of P (frictional power loss)

It has been observed that with the value of 0.0628 MJ, power consumption is maximum for base oil alone. It decreases appreciably for admixtures; 0.0505 MJ for g-C_3N_4, 0.0458 MJ for

m-$LaVO_4$, and 0.0353 MJ for g-C_3N_4/m-$LaVO_4$ (**Table 6.1**). Thus, minimum energy consumption was observed for the nanocomposite (g-C_3N_4/m-$LaVO_4$).

Table 6.1. Frictional power loss (P) for various nano additives at 0.05 percent w/v concentration of additives in PO

S.N.	Additives	Power Consumption (MJ)	Reduction in Power Consumption	% Reduction in Power Consumption
1.	PO	0.0628	____	____
2.	g-C_3N_4	0.0505	0.0123	19.6
3.	m-$LaVO_4$	0.0458	0.0170	27.1
4.	g-C_3N_4/m-$LaVO_4$	0.0353	0.0275	43.8

6.4.3. Characterization of worn surfaces

SEM and AFM of the worn surface of the AISI 52100 steel ball lubricated with plain paraffin oil in the presence and absence of additives at 0.050 percent w/v after the antiwear test were recorded for the morphological analysis. **Fig. 6.10(a-d)** shows SEM micrographs, the steel surface in the presence of paraffin oil alone is highly corrugated. In contrast, admixtures of nano additives with paraffin oil significantly enhance the smoothness of the steel surface. The antiwear behavior of the examined admixtures is directly related to the extent of the steel surface improvement. In the inset view **Fig.6.10(a-d)**, the MWD values are provided; PO (0.735 mm), g-C_3N_4; (0.667 mm), m- $LaVO_4$ (0.572 mm), and g-C_3N_4/m-LaVO4 (0.451 mm). The worn steel surface smoothness matches the order of MWD.

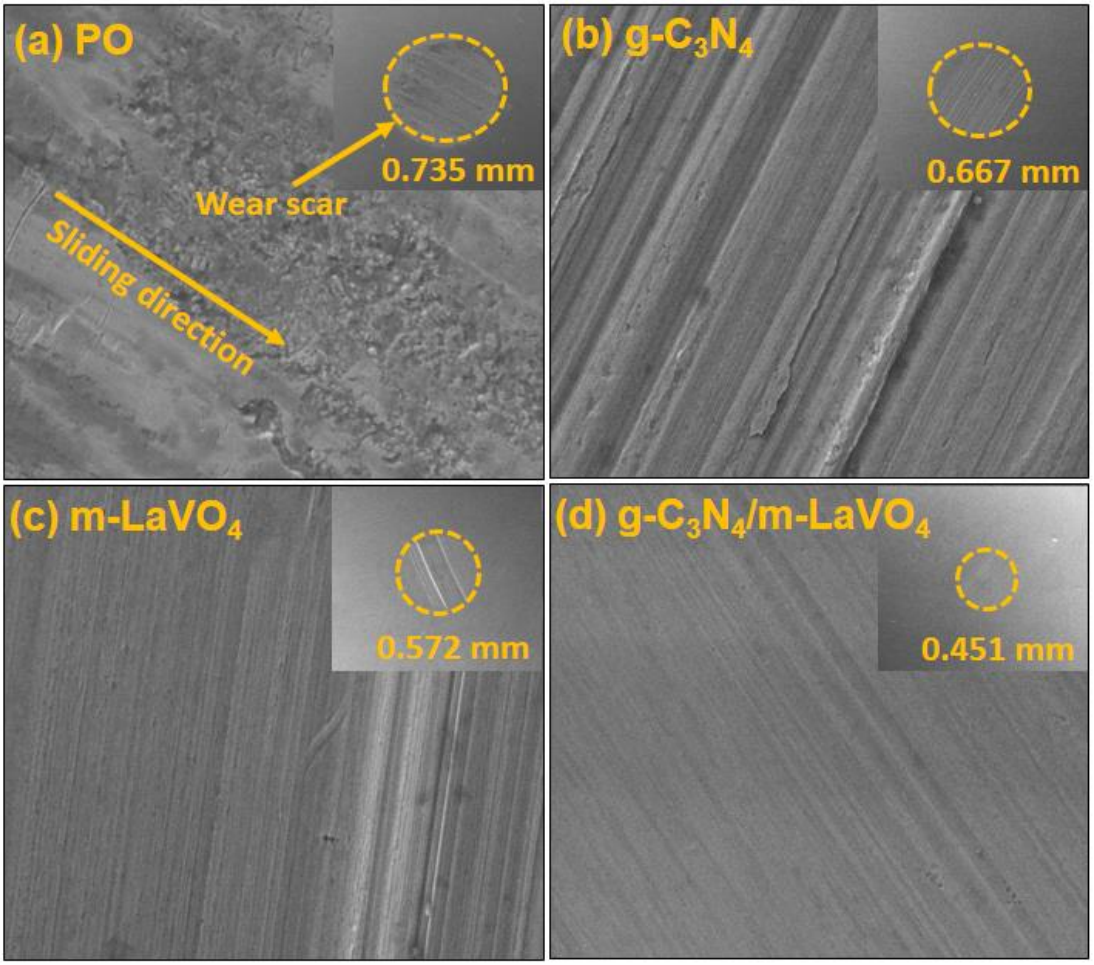

Fig. 6. 10. (a-d) SEM images at 2.00K× magnification after ASTM D4172 test depicting wear scar surface lubricated with PO alone and its blends with additives at 0.05 % w/v concentration (inset: full view showing 100× wear scar)

The EDX spectra of the worn steel surface in the presence of g-C_3N_4, m-$LaVO_4$, and the composite have been shown in **Fig. 6.11**, indicating the presence of constituent elements, which validates the adsorption of additives on the worn steel surface.

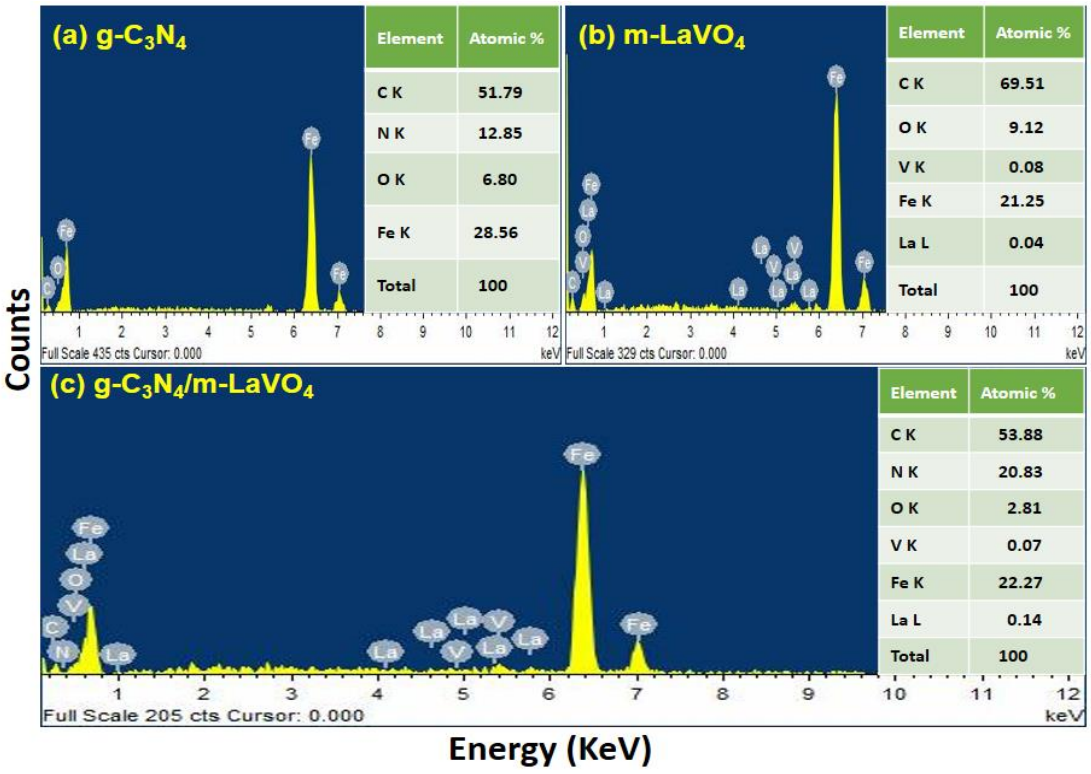

Fig. 6. 11. EDX spectrum of worn surfaces lubricated with additives g-C_3N_4, m-$LaVO_4$ and g-C_3N_4/m-$LaVO_4$

Fig. 6.12 (a-d) depicts 3*D* AFM photographs of the wear scar and surface roughness data (area roughness; Sq, line roughness; Rq). A significant decrease has been noticed in the values of Sq and Rq from base oil to the admixtures. It is visible that the surface in the case of the nanocomposite (g-C_3N_4/m-$LaVO_4$) becomes more even compared to g-C_3N_4 and m-$LaVO_4$.

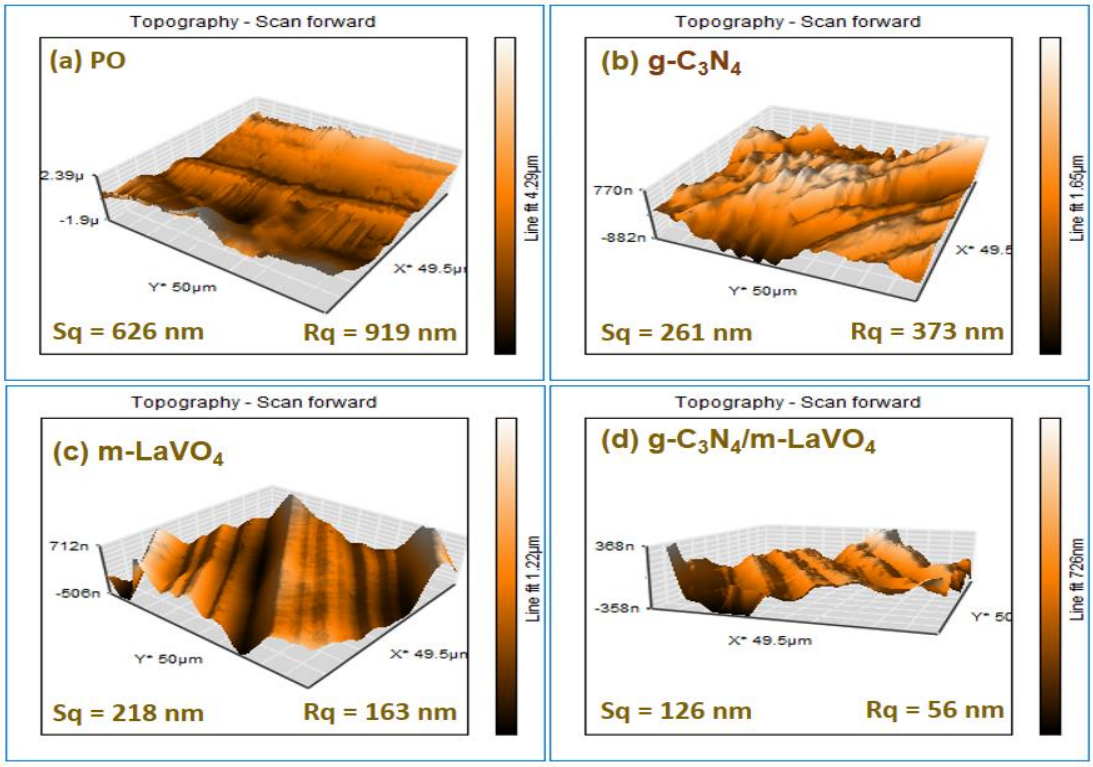

Fig. 6.12. 3D AFM pictures of worn surface lubricated with PO in the presence and absence of additives at 0.05 %w/v concentration after ASTM D4172 test (a) PO, (b) nanosheets, (c) m-nanoparticles, (d) composite

The XPS of worn steel surface lubricated with composite (g-C_3N_4/m-$LaVO_4$) after the ASTM D4172 test has been used to identify the chemical states of the individual constituents of the *in situ* generated tribofilm. The core-level spectra of C 1s, O 1s, N 1s, V 2p, La 3d, and Fe 2p have been shown in **Fig. 6.13(a-f)** using the peak fit software. The C1s spectrum reveals two peaks corresponding to C–C/C=C and N-C=N at 284.8 and 288.7 eV, respectively, **Fig. 6.13a**. [Singh et al. (2021), Kavita et al. (2020)]. Hence, the chemical state of C bonded to C and N remains almost unaffected in the tribofilm. The O1s spectrum, **Fig. 6.13b**, shows two peaks with binding energies 529.6 and 532.1 eV corresponding to the Fe-O (Fe_2O_3) and V-O bond (VO_4^{3-}), respectively [He et al. (2014), Kavita et al. (2020)]. The N 1s spectrum, **Fig.**

6.13c, reveals three peaks at binding energies 398.6, 399.7, and 400.6 [Tan et al. (2017)]. In the V 2p core-level spectrum, **Fig. 6.13d**, peaks with binding energies 516.6 and 523.5 eV have been identified for V $2p_{3/2}$ and V $2p_{1/2}$, respectively, indicating the presence of V^{+5} ion [Li et al. (2022)]. **Fig. 6.13e** portrays La 3d spectrum, where peaks with binding energies 834.9 and 838.3 correspond to La $3d_{5/2}$ and peaks at 851.8 and 855.7 eV correspond to La $3d_{3/2}$ [Li et al. (2022)].

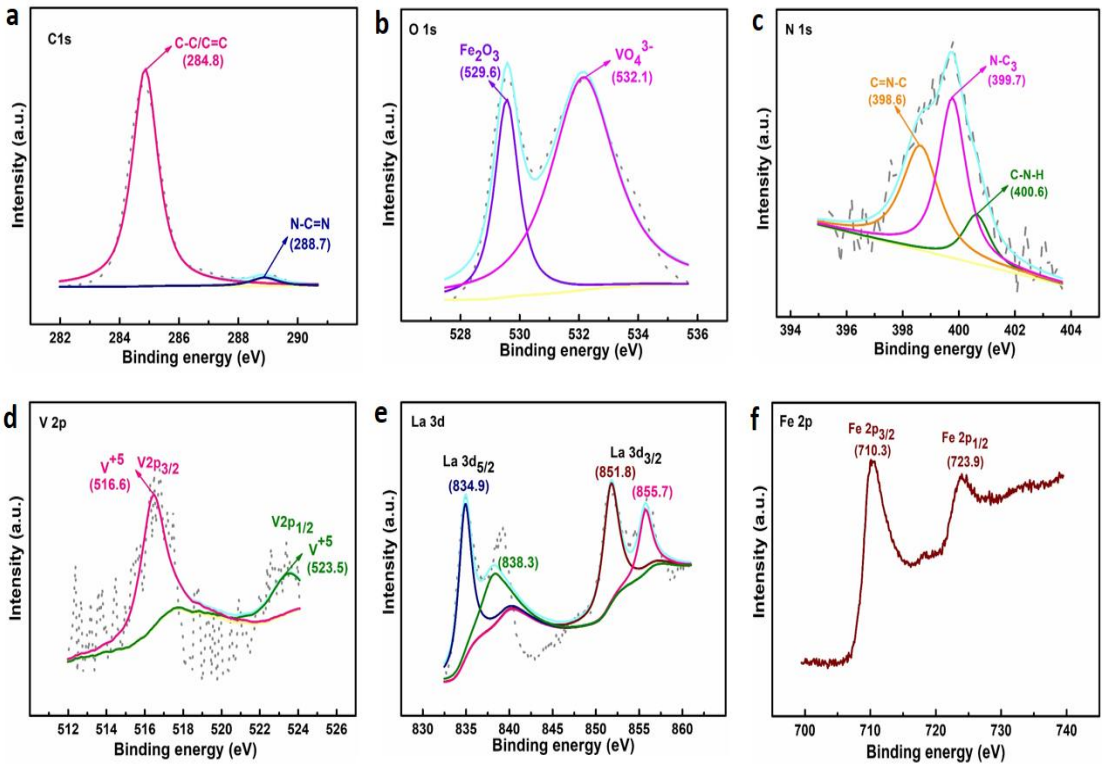

Fig. 6.13. Deconvoluted C 1s, O 1s, N 1s, V 2p, La 3d, and Fe 2p XPS spectra of the wear track lubricated using nanocomposite g-C_3N_4/m-$LaVO_4$ after ASTM D4172 test

In general, the binding energies of all the peaks discussed above remain almost unaffected after the antiwear test though their intensities are a bit lowered; therefore, the chemical states of the

elements have not changed. In the Fe 2p spectrum, **Fig. 6.13f**, two peaks could be observed at binding energies 710.3 (Fe $2p_{3/2}$) and 723.9 eV (Fe $2p_{1/2}$), showing the formation of Fe_2O_3 [Kavita et al. (2020), Kavita et al. (2022), Verma et al. (2018), Verma et al. (2020a), Kumar et al. (2020a)]. Hence, tribofilm can be inferred to be made up of adsorbed organic moieties of g-C_3N_4, V_2O_5, La_2O_3, and tribochemically oxidized Fe_2O_3.

6.4.4. Tribo-chemistry and mechanism of lubrication

It has been observed from the above discussion that the lubricant additives cling to the adjacent moving surfaces and culminate into the formation of a tribofilm *in situ* under the test conditions of ASTM D4172 that bears the load. The efficacy of the additives is related to the feasibility of durable, tenacious tribofilm formation. The presence of V_2O_5 and La_2O_3 in the tribofilm formed by the composite g-C_3N_4/m-$LaVO_4$ supports the observed tribological data.

The magnificent performance of the nanocomposite g-C_3N_4/m-$LaVO_4$ is mainly attributed to mutualistic interactions between g-C_3N_4 nanosheets and m-$LaVO_4$ nanoparticles. Indeed, the lamellar heteropolymeric structure of the g-C_3N_4 nanosheets facilitated sliding motion. The m-$LaVO_4$ nanoparticles decorated on nanosheets helped in the segregation of the nanosheets to control their re-stacking [Shukla et al. (2020)]. In addition, the nanoparticles reinforced the nanosheets, averted their agglomeration [Shukla et al. (2020)], enhanced the dispersibility in the base lube [Shukla et al. (2020)], and improved the tenacity of g-C_3N_4. The g-C_3N_4 nanosheets, in turn, prevented the agglomeration of nanoparticles, too. The other modalities of nanoparticles, like their nano-bearing behavior, mending of the proximal surfaces by tribosinterization, and polishing the worn surface, might have further facilitated sliding action [Shukla et al. (2020)]. **Fig. 6.14** displays the schematic representation of the lubrication mechanism of binary nanocomposite g-C_3N_4/m-$LaVO_4$.

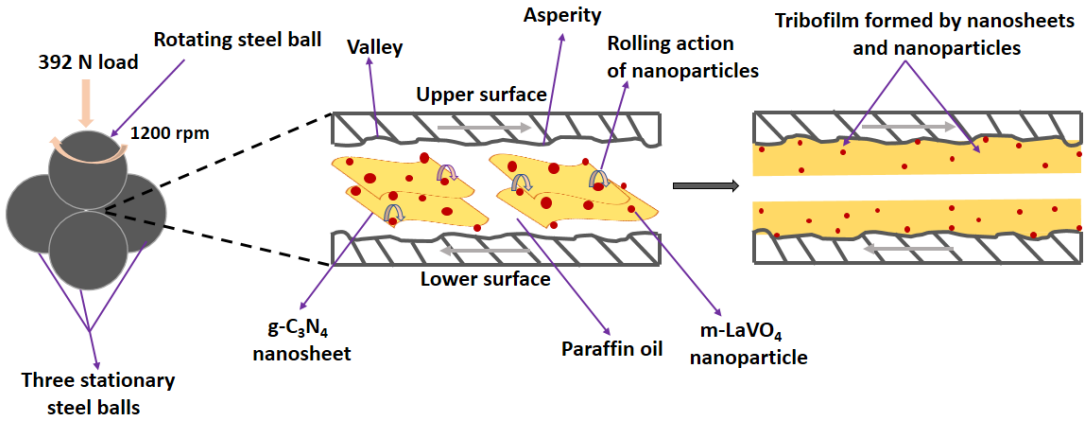

Fig. 6.14. Diagrammatic depiction of the proposed lubrication mechanism in the presence of PO blended with nanocomposite (g-C_3N_4/m-$LaVO_4$)

6.5. Conclusions

The graphitic carbon nitride, g-C_3N_4, was prepared by heating melamine, followed by ultrasonication. A solution combustion method has been used to prepare m-$LaVO_4$ nanoparticles using glycine as fuel. Further, the preparation of nanocomposite (g-C_3N_4/m-$LaVO_4$) was achieved by ultrasonication. FE-SEM, TEM, and HR-TEM were used to study the morphology of the additives. XRD, EDX, and FT-IR further characterized the additives. The m-$LaVO_4$ nanoparticles and g-C_3N_4 nanosheets are bonded together by weak physical interactions. The dispersions of the additives were found to be appreciably stable, as studied by UV/visible spectroscopy. The tribological parameters, MWD, COF, and load-carrying capacity of the synthesized additives were obtained from ASTM D4172 and ASTM D5183 tests at 0.05%w/v concentration. Undoubtedly, the nanoparticles and nanosheets show high tribological activity, but the composite shows an enormous increase in activity due to strong synergistic interactions. The SEM and AFM studies of the wear scar surface authenticate the

observed activity. XPS studies reveal that the tribofilm is composed of adsorbed organic moieties of g-C_3N_4, V_2O_5, La_2O_3, and tribochemically oxidized Fe_2O_3. Thus, the nanocomposite establishes itself as a potential wear and friction modifier for lubricating systems.